

## Article

# Nonlinear Transport and Magnetic/Magneto-Optical Properties of $\text{Co}_x(\text{MgF}_2)_{100-x}$ Nanostructures

Sergey A. Ivkov <sup>1</sup>, Konstantin A. Barkov <sup>1</sup>, Evelina P. Domashevskaya <sup>1</sup> , Elena A. Ganshina <sup>2</sup> , Dmitry L. Goloshchapov <sup>1</sup>, Stanislav V. Ryabtsev <sup>1</sup>, Alexander V. Sitnikov <sup>3</sup> and Pavel V. Seredin <sup>1,\*</sup> 

<sup>1</sup> Department of Solid State Physics and Nanostructures, Faculty of Physics, Voronezh State University, Universitetskaya pl. 1, 394018 Voronezh, Russia

<sup>2</sup> Department of Magnetism, Faculty of Physics, Lomonosov Moscow State University, Leninskiye Gory B 1-2, GSP-1, 119991 Moscow, Russia

<sup>3</sup> Department of Solid State Physics, Faculty of Radio Engineering and Electronics, Voronezh State Technical University, 14 Moskovsky Ave., 394026 Voronezh, Russia

\* Correspondence: paul@phys.vsu.ru

**Abstract:** The aim of this work was to comprehensively study the effect of the variable atomic composition and structural-phase state of  $\text{Co}_x(\text{MgF}_2)_{100-x}$  nanocomposites on their nonlinear transport and magnetic/magneto-optical properties. Micrometer-thick nanocomposite layers on glass substrates were obtained by means of ion-beam sputtering of a composite target in the argon atmosphere in a wide range of compositions ( $x = 16\text{--}59$  at.%). Using a low metal content in the nanocomposite, magnesium fluoride was kept in the nanocrystalline state. As the metal content increased, nanocrystalline cobalt was formed. The value of the resistive percolation threshold,  $x_{\text{per}} = 37$  at.%, determined from the concentration dependences of the electrical resistance of the nanocomposites coincided with the beginning of nucleation of the metallic nanocrystals in the  $\text{MgF}_2$  dielectric matrix. The absolute value of the maximum negative magnetoresistive effect in the nanocomposites was 5% in a magnetic field of 5.5 kG at a Co concentration of  $x = 27$  at.%.



**Citation:** Ivkov, S.A.; Barkov, K.A.; Domashevskaya, E.P.; Ganshina, E.A.; Goloshchapov, D.L.; Ryabtsev, S.V.; Sitnikov, A.V.; Seredin, P.V. Nonlinear Transport and

Magnetic/Magneto-Optical Properties of  $\text{Co}_x(\text{MgF}_2)_{100-x}$  Nanostructures. *Appl. Sci.* **2023**, *13*, 2992. <https://doi.org/10.3390/app13052992>

Academic Editor: Roberto Bergamaschini

Received: 30 January 2023

Revised: 22 February 2023

Accepted: 22 February 2023

Published: 26 February 2023



**Copyright:** © 2023 by the authors. Licensee MDPI, Basel, Switzerland. This article is an open access article distributed under the terms and conditions of the Creative Commons Attribution (CC BY) license (<https://creativecommons.org/licenses/by/4.0/>).

**Keywords:** nanocomposites; nanocrystals; magnetoresistance; percolation threshold; impedance hodograph; magneto-optical properties; transversal Kerr effect

## 1. Introduction

The reduction in the size of functional devices of modern electronics has led to a number of problems associated not only with technological limitations, but also with the fact that new physical phenomena that are characteristic of nanoscale objects begin to operate. When working with small electronic devices, quantum size effects become decisive. This also has its advantages, as opportunities arise in the development of subminiature transistors, memory cells, and magnetic and electric field sensors.

One of the studied effects of nanosized objects is the effect of tunneling magnetoresistance in metal–dielectric composite films, which has been studied for several decades [1–11]. It should be noted that systems based on cobalt have high values of the TMR effect [5–11].

Various scientific groups have carried out studies evaluating the effect of self-organization on the magnetic properties of nanomaterials. The manifestation of properties in nanocomposites depends on the composition and concentration [12–16]. In this regard, the study of their structural, electrophysical, magnetic, and magneto-optical properties is of interest.

In this case, the concept of the percolation threshold is introduced. The percolation threshold denotes the amount of the metal component at which a sharp change occurs in the resistance of the nanocomposite, changing its conductivity. It is the region of the percolation threshold that represents the most interesting range of studies. In nanocomposites with compositions near the percolation threshold, special physical properties such as tunneling magnetoresistance can be observed. The most effective and simplest method for obtaining

such granular nanocomposites is the ion-plasma sputtering method. Iron, cobalt, nickel, and alloys of these elements are often used as the metal components of granular nanocomposites. Oxides of aluminum, silicon, magnesium, and titanium are often used as dielectric components. Unique alloys and compounds are used, but do not always give good results [17–19].

Articles [20–24] present the results of studies on the influence of the formation of the structure of granular nanocomposites on the effect of tunneling magnetoresistance. Oxide and oxide-free matrices were used to obtain nanocomposites. The data obtained led us to conclude that the best characteristics in terms of the maximum value of magnetoresistance were demonstrated using oxide-free matrices.

It is important to note that high TMR Co multilayer-based device technology requires high-vacuum deposition equipment. This is due to the need to obtain a high-quality interface between the metal–dielectric layers. In the case of manufacturing nanogranular composites, less expensive equipment is required [17].

The purpose of this work was to perform a comprehensive study of the influence of the atomic composition and structural-phase state of  $\text{Co}_x(\text{MgF}_2)_{100-x}$  nanocomposites on their nonlinear transport and magneto/magneto-optical properties. In this article, we link our previous studies of the phase composition and structure of granular  $\text{Co}_x(\text{MgF}_2)_{100-x}$  nanocomposites [25] with their electrical and magnetic properties.

## 2. Materials and Methods

$\text{Co}_x(\text{MgF}_2)_{100-x}$  nanocomposite films with different contents of metallic cobalt (Co) in the  $\text{MgF}_2$  dielectric matrix were obtained on glass substrates via ion-beam sputtering [17]. Film deposition was conducted in a vacuum chamber ( $10^{-6}$  Torr) filled with Ar (purity 99.992%) up to a total gas pressure of  $8 \times 10^{-4}$  Torr. A magnetic system consisting of permanent magnets, a magnetic circuit, and an anode was used as a source of ion-beam sputtering. Argon ionization was carried out in the magnet gap in the immediate vicinity of the anode. A high magnetic field strength (80 kA/m) was created in this magnet gap. In turn, a positive bias (4 kV) was applied to the anode. The perpendicular configuration of the magnetic and electric fields in the area of the magnetic gap led to the emergence of an independent glow discharge. Under the action of an electric field,  $\text{Ar}^+$  was ejected from the plasma, creating a high-energy ion beam, which was directed at the target. The optimal plasma current was  $\sim 170 \mu\text{A}$ . This mode ensured a deposition rate of nanocomposite films of  $\sim 1.5 \mu\text{m/h}$ .

The crystal structures of the  $\text{Co}_x(\text{MgF}_2)_{100-x}$  nanocomposites were determined on a diffractometer using  $\text{CoK}\alpha$  radiation (DRON 4-07). Samples were collected at an accelerating voltage of 29 kV in the X-ray tube with an anode current of 26 mA. The intensity of the scattered X-rays was recorded in continuous scanning mode with a detector rotation speed of 1 deg./min. in the angle range  $2\Theta$  ( $10$ – $100^\circ$ ) according to the Bragg–Brentano geometry. The phase composition was determined using the International Center for Diffraction Data's PDF Release 2012 (ICDD).

The Co concentration in atomic % and the thicknesses of film composites were determined using electron probe X-ray spectral microanalysis on an attachment to a JEOL JSM-6380LV scanning electron microscope (Japan) with an error not exceeding 1.5% of the content of the measured element at beam energies of 5 keV.

The tunneling magnetoresistance effect was studied using the four-probe method on an ECOPIA HMS-3000 instrument. The maximum value of the voltage was 10 volts. The device package included a certified magnetic attachment with a magnetic induction of  $B = 5.5 \text{ kG}$ .

The impedance of the investigated samples was measured by applying alternative signals using an Elins Z-1500J impedance meter. These studies were carried out at room temperature in the frequency range from 1 mHz to 3 MHz. The amplitude of the alternating measuring signal did not exceed 100 mV. The measurement error did not exceed 5%. The analysis of the impedance spectra was carried out within the framework of a model of serially connected parallel equivalent circuits using the procedure for processing experimental data with modern software.

To study the magnetic properties of nanocomposites, we used an automated Lake Shore 7404 VSM vibrating magnetometer with a sensitivity of  $10^{-5}$ – $10^{-7}$  G\*cm<sup>3</sup>. Studies of the magneto-optical response were carried out on an automated magneto-optical spectrometer in the incident light energy range E from 0.5 to 4 eV at room temperature. The amplitude of the applied alternating magnetic field reached 3 kOe. An important feature of this method is the study of the equatorial Kerr effect when the object is in a variable magnetic field. This method has very high accuracy relative to the intensity of light (up to  $10^{-5}$ ).

### 3. Results

#### 3.1. Structure and Composition of Granular Nanocomposites $\text{Co}_x(\text{MgF}_2)_{100-x}$

The thicknesses of granular nanocomposites  $\text{Co}_x(\text{MgF}_2)_{100-x}$  obtained by ion-beam sputtering are presented in Table 1.

**Table 1.** The atomic concentration and thicknesses of the investigated samples.

Co, x (at.%)	16	19	27	32	37	42	47	50	55	59
d, $\mu\text{m}$ .	0.70	0.95	1.50	1.50	2.25	2.00	2.60	2.20	1.80	2.40

The thicknesses of the investigated films of the nanocomposites on glass substrates varied in the range of 0.7–2.6  $\mu\text{m}$  in accordance with an increase in the Co metal content (x at.%) in the range  $x = 16$ –59 at.%.

In Figure 1, we reproduce the diffraction patterns of nanocomposite samples from our previous work [25] with different cobalt content (x at.%), which is shown to the right of each diffraction pattern. It can be seen that at a low content ( $x < 27$  at.%), amorphous cobalt clusters distributed in the medium of nanocrystals of the  $\text{MgF}_2$  dielectric component only yield a small increase in the intensity in the region  $2\theta \sim 55^\circ$ , and the main reflections from the  $\text{MgF}_2$  nanocrystalline phase form broad lines (110) and (220). However, with an increase in the metal content in the NCs, Co nanocrystals of hexagonal syngony at  $x = 42$  at.% begin to form on the glass substrates (Figure 1), while the  $\text{MgF}_2$  dielectric matrix becomes X-ray amorphous-like and its reflections disappear, giving way to a wide halo in the  $2\theta \sim 32^\circ$  region. The average size of these cobalt nanocrystals, calculated by the Debye–Scherrer formula, increases from 10 nm at  $x = 42$  at.% to 20 nm at  $x = 59$  at.%.  $\text{MgF}_2$  nanocrystals of the dielectric matrix in these composites have slightly increased interplanar distances  $d_{110}$  and  $d_{220}$  compared to the reference microcrystalline  $\text{MgF}_2$  [25].

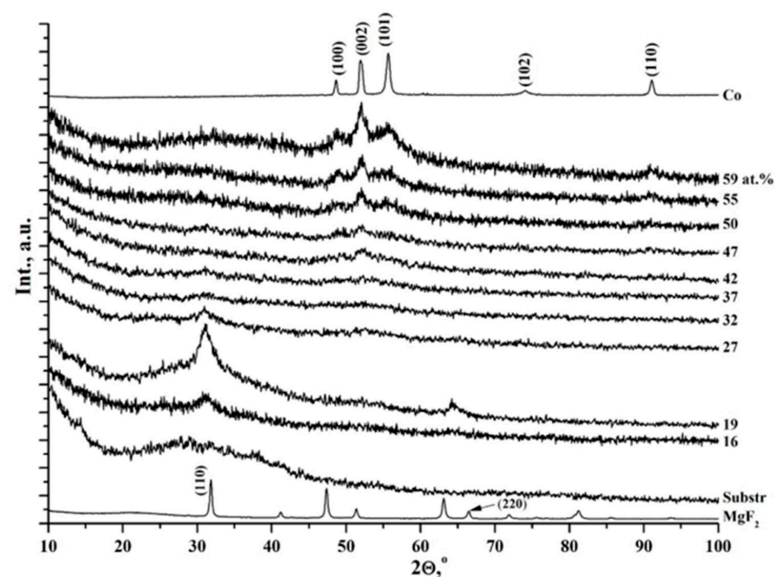


**Figure 1.** XRD patterns of  $\text{Co}_x(\text{MgF}_2)_{100-x}$  nanocomposites of various compositions on glass substrates [25].

### 3.2. Concentration Dependences of Electrical Resistance and Magnetoresistive Effects

Studies of the concentration dependence of electrical resistance presented in Figure 2a and Table 2 show that at a low cobalt content in the range of  $x = 16\text{--}27$  at.%, the resistance of the nanocomposites reaches  $10^7\text{--}10^6$  Ohm, which is characteristic for dielectrics, while in the interval of  $x = 47\text{--}59$  at.%, the resistance drops to a few ohms or even less, as is typical for metals. In the transition interval of  $x = 32\text{--}42$  at.% corresponding to the formation of cobalt nanocrystals, there is a sharp drop in resistance by 4–5 orders of magnitude, corresponding to the percolation threshold at  $x_{\text{per}} = 37$  at.% (Figure 2a).

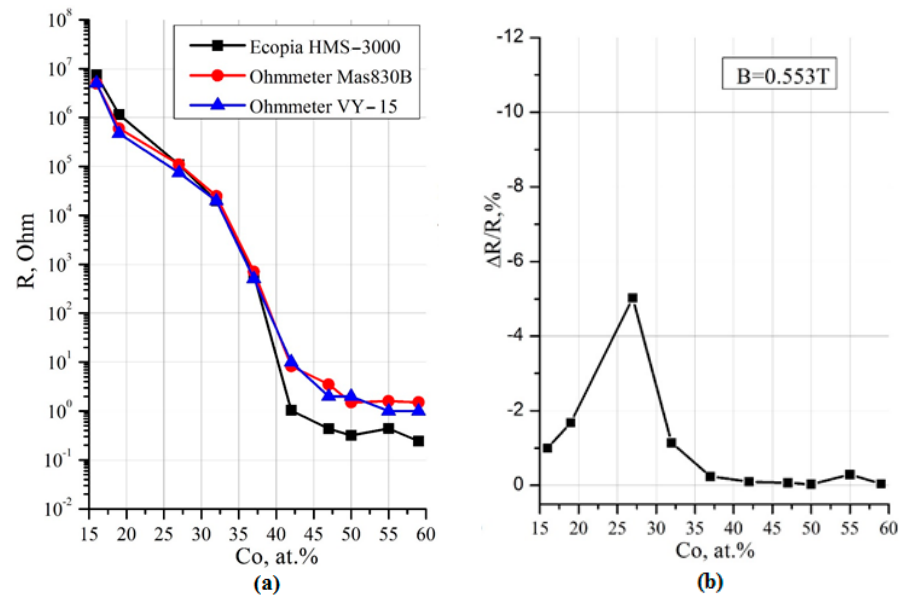


**Figure 2.** Concentration dependences of electrical resistance (a) and magnetoresistance (b) of  $\text{Co}_x(\text{MgF}_2)_{100-x}$  nanocomposites.

**Table 2.** Concentration dependence of the total electric resistance R and capacitance C of the nanocomposites  $\text{Co}_x(\text{MgF}_2)_{100-x}$ .

$\text{Co}_x, x$ (at.%)	16	19	27	32	37	42	47	50	55	59
R, Ohm	$1 \times 10^7$	$1.6 \times 10^6$	$15 \times 10^4$	$12 \times 10^4$	830	20	2	2	2	2
C, f	$3 \times 10^{-12}$	$3 \times 10^{-12}$	$4 \times 10^{-12}$	$6 \times 10^{-12}$	$2 \times 10^{-9}$	-	-	-	-	-

The absolute values of the tunneling magnetic resistance (TMR) of these nanocomposites were determined in accordance with the expression:

$$\frac{\Delta R}{R(0)} = \frac{(R(H) - R(0))}{R(0)} * 100\%, \tag{1}$$

where  $R(H)$  is the resistance of the sample in the presence of an external magnetic field  $H$ , and  $R(0)$  is the resistance of the composite in the absence of an external magnetic field.

Figure 2b shows the concentration dependence of the magnetoresistive effect in the form of negative TMR values for the samples of the  $\text{Co}_x(\text{MgF}_2)_{100-x}$  system measured in a magnetic field with induction  $B = 5.5$  kG. This shows that as the cobalt percentage increases to  $x = 27$  at.%, there is a sharp increase in TMS to a maximum value  $\Delta R/R(0) = 5\%$ . As the proportion of the metal phase ( $x > 27$  at.%) increases further, the TMR effect gradually drops to zero in the region of the percolation threshold. Such a picture is characteristic of many systems of metal-dielectric nanocomposites [26].

### 3.3. Capacitive/Inductive Nature of the Resistance of $\text{Co}_x(\text{MgF}_2)_{100-x}$ Nanocomposites According to Impedance Data

Impedance spectroscopy is one of the most accessible methods for studying electro-physical processes [27,28].

$$\text{Impedance } Z = R - i \frac{1}{\omega C}, \quad (2)$$

where  $i = \sqrt{-1}$ ,  $\omega$  is the cyclic frequency, and  $C$  is the total capacitance of the composite.  $Z' = R$  is the real resistance component, and  $Z'' = 1/\omega C$  is the imaginary resistance component. The hodograph of the impedance  $Z$  (impedance diagrams) is a graphical dependence of the imaginary component of the impedance  $Z''$  on the real  $Z'$ .

For  $\text{Co}_x(\text{MgF}_2)_{100-x}$  nanocomposites, impedance data show two different types of hodographs before and after the percolation threshold (Figure 3). On the hodograph for a nanocomposite with a cobalt content up to the percolation threshold of  $x = 32$  at.%, a semicircle is observed, which corresponds to the typical behavior of the RC chain of metal clusters in a dielectric matrix. At the percolation threshold of  $x = 37$  at.%, a rectilinear section appears on the hodograph semicircle, which takes the form of an inclined line at  $x = 42$  at.%, and then, as  $x$  increases beyond the percolation threshold, the hodograph becomes a vertical line, indicating the metallic nature of the ohmic conduction.

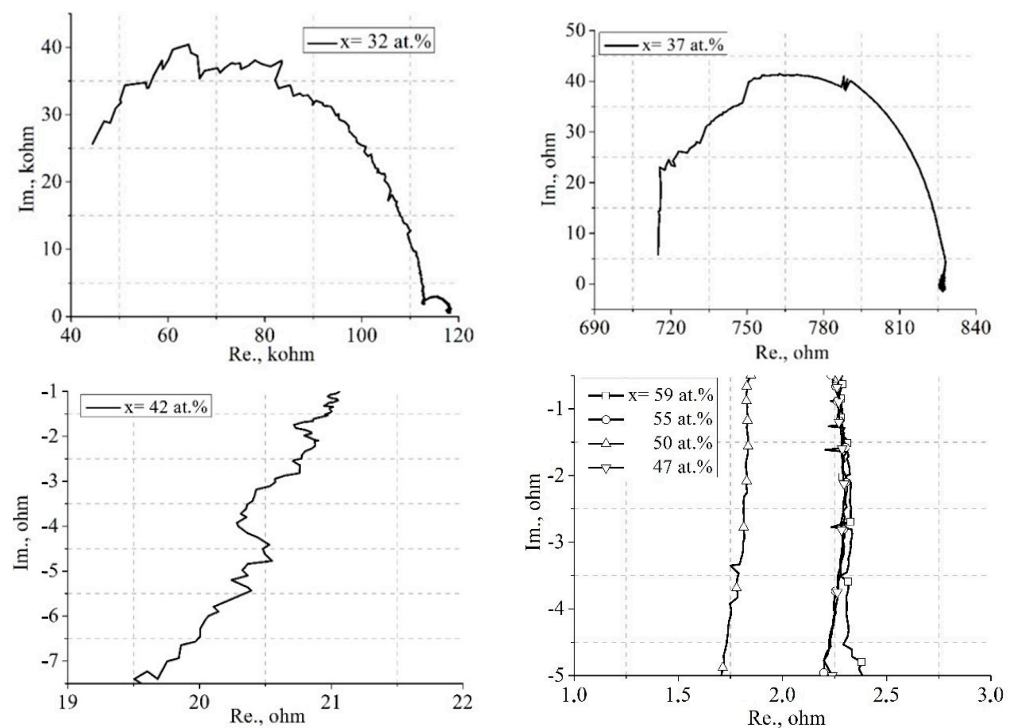


**Figure 3.** Impedance diagrams (hodographs) for nanocomposites  $\text{Co}_x(\text{MgF}_2)_{100-x}$  of different compositions ( $32 \leq x \leq 59$ ).

The resistance and capacitance values of the nanocomposites, according to the impedance data given in Table 2, show that the capacitance of the nanocomposites in the pre-percolation region does not exceed several units of picofarads. Only in the region of the percolation threshold ( $x_{\text{per}} = 37$  at. %) does the capacitance increase by three orders of magnitude up to two nanofarads. This increase in the capacitance value is due to the beginning of the formation of metallic nanocrystals and the remaining dielectric interlayers between them.

### 3.4. Magneto-Optical and Magnetic Properties of $\text{Co}_x(\text{MgF}_2)_{100-x}$ Nanocomposites

The magneto-optical Kerr effect changes the intensity of light reflected by a sample magnetized perpendicular to the plane of incidence of light [12]. The value and sign of

TKE are defined as the ratio of the difference between the intensities of the light reflected by the sample in the magnetized ( $I$ ) and demagnetized ( $I_0$ ) states to the light intensity  $I_0$ :

$$\delta = \frac{I - I_0}{I_0} = \frac{\Delta I}{I_0} \quad (3)$$

The absolute value of TKE depends on the amount of the metal phase in the composite. Its increase leads to an increase in the TKE modulus, which reaches the maximum at a concentration corresponding to the percolation threshold.

Figure 4 shows the concentration dependences of the transversal Kerr effect (TKE) for  $\text{Co}_x(\text{MgF}_2)_{100-x}$  nanocomposites at three values of the incident light photon energy of  $E = 1.14$  eV,  $1.97$  eV, and  $3.17$  eV. The maximum absolute value in the concentration dependences of TKE is observed at the energy values of  $E = 1.97$  eV and  $3.28$  eV. This maximum in the concentration dependence of TKE coincides with the electrical resistive percolation threshold  $x_{\text{per}} = 37$  at.%.

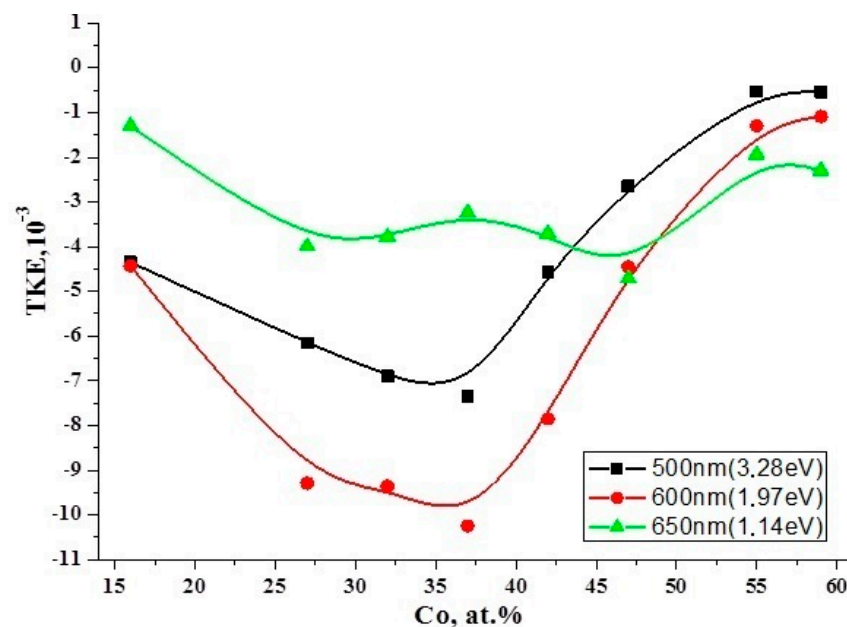


**Figure 4.** Concentration dependences of the transversal Kerr effect (TKE) for nanocomposites  $\text{Co}_x(\text{MgF}_2)_{100-x}$  at different values of incident light energy.

In contrast, the concentration dependences of TKE in the NC  $(\text{CoFeZr})_x(\text{MgF}_2)_{100-x}$  system, which we obtained earlier from [29,30], showed two maxima, one of which corresponded to the formation of hexagonal nanocrystals of the  $\text{CoFeZr}$  alloy based on  $\alpha$ -Co ( $x = 30$  at.%). The second at  $x = 45$  at. % corresponded to the transition of the hexagonal structure to the cubic structure  $\alpha$ -Fe.

During the MO study of our  $\text{Co}_x(\text{MgF}_2)_{100-x}$  system, we obtained two  $x$  values with maxima of the TKE concentration dependence at the lowest incident light energy  $E = 1.14$  eV: the first value,  $x = 27$  at.%, corresponds to the maximum of the magnetoresistive effect (Figure 2b), and the second value,  $x = 45$  at.%, is close to the threshold of impedance; the hodograph changes from a capacitive to an ohmic character at  $x = 42$  at.% in Figure 3.

Thus, magneto-optical spectra respond to changes in the composition, atomic structure, and magnetic order of complex heterophase systems.

In Figure 5, we present the dependences of the magnetizations on the magnetic field arising parallel and perpendicular to the sample plane, which show the first appearance of a hysteresis loop with a coercive force of  $H_c \approx 18$  Oe in a  $\text{Co}_{32}(\text{MgF}_2)_{68}$  sample with a cobalt content of  $x = 32$  at.%. In this case, saturation magnetization has different values.

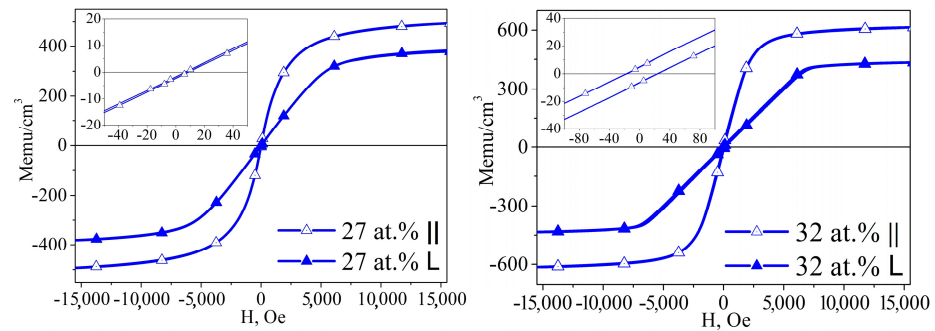


**Figure 5.** The M–H loop for NC  $\text{Co}_{32}(\text{MgF}_2)_{68}$  and for NC  $\text{Co}_{27}(\text{MgF}_2)_{73}$ , where the solid delta shows the M–H loop with an out-of-plane magnetic field, and the open delta presents the in-plane M–H loop.

We assume that there is magnetic anisotropy in granular nanocomposites, which is not related to structural properties but is determined by internal stresses in the nanocomposite. During the deposition of nanocomposites on a substrate, both internal and microscopic stresses in the sample volume and macroscopic stresses at the nanocomposite–substrate interface are allowed to appear. It can also be assumed that micro- and macrostresses in nanocomposites should affect the magnitude and direction of the anisotropy fields of both individual ferromagnetic granules and the material as a whole. Parallel tensile microstress increases the in-plane anisotropy field in the direction perpendicular to the sample axis. Compressive microstress reduces the magnitude of the anisotropy field in the perpendicular direction.

We do not exclude the influence of the texture of nanocomposites on their magnetic properties. The formation of composites under artificially created conditions that specify a certain predominant orientation of granules or clusters should lead to the creation of textures and, as a result, to magnetic anisotropy in the nanocomposite [31,32].

In the future, we plan to study the structure of these granules using a transmission electron microscope and conduct studies of magnetostrictive anisotropy in the nanocomposite.

This means that the magnetic percolation threshold in the  $\text{Co}_x(\text{MgF}_2)_{100-x}$  NC system at  $x_{\text{fm}} = 32$  at.% occurs before the resistive percolation threshold  $x_{\text{per}} = 37$  at.% due to the exchange interaction between electrons and spins non-contacting metal nanocrystals of small sizes.

At a low content of metallic cobalt,  $x < 27$  at.%, NCs are superparamagnetic ( $H_c = 0$ ). As the cobalt content rises, the coercive force increases to  $H_c \approx 95$  Oe (Figure 6).

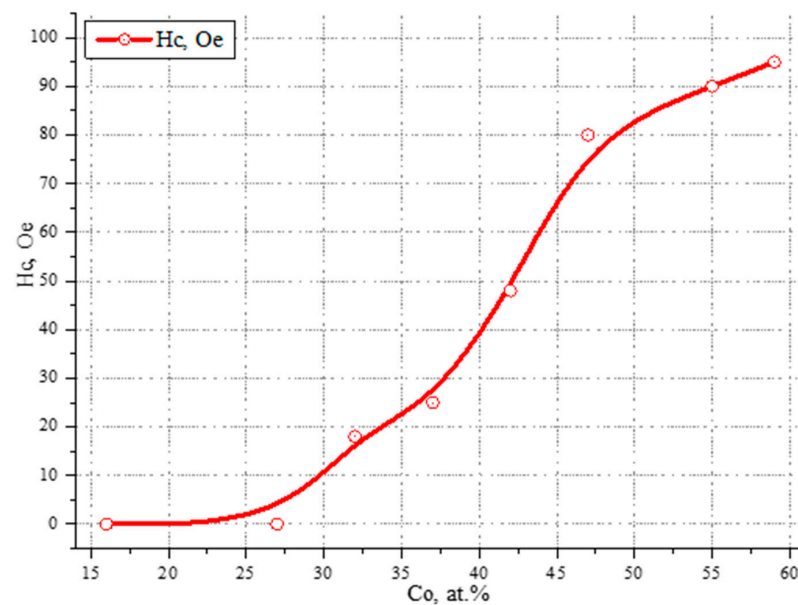


**Figure 6.** Concentration dependence of the coercive force ( $H_c$ ) for  $\text{Co}_x(\text{MgF}_2)_{100-x}$  nanocomposites.

#### 4. Conclusions

In this work, the influence of the atomic composition and structural-phase state of  $\text{Co}_x(\text{MgF}_2)_{100-x}$  nanocomposites on their nonlinear transport and magneto/magneto-optical properties was studied.

We demonstrated that in  $\text{Co}_x(\text{MgF}_2)_{100-x}$  nanocomposites of variable composition obtained by ion-plasma sputtering, nanocrystals of various phases are formed depending on the composition. Under a low metal content in the nanocomposite ( $x < 42$  at.%), magnesium fluoride is in the nanocrystalline state. As the metal content increases, nanocrystalline cobalt is formed ( $x > 42$  at.%). Our article showed that the value of the percolation threshold of nanocomposites ( $x_{\text{per}} = 37$  at.%), determined from the concentration dependences of the electrical resistance of nanocomposites, coincides with the beginning of nucleation of hexagonal cobalt nanocrystals in the  $\text{MgF}_2$  dielectric matrix.

It was shown that the absolute value of the maximum negative magnetoresistive effect in the studied nanocomposites is 5% in a field of 5.5 kG at a cobalt concentration of  $x = 27$  at. %, up to the percolation threshold. The threshold of magnetic percolation in the  $\text{Co}_x(\text{MgF}_2)_{100-x}$  NC system occurs at  $x_{\text{fm}} = 32$  at.% along with the appearance of a hysteresis loop and the coercive force of  $H_c \approx 18$  Oe, i.e., up to the resistive percolation threshold  $x_{\text{per}} = 37$  at. %, as a result of the exchange interaction. At a low content of metallic cobalt,  $x < 27$  at.%, nanocomposites are superparamagnetic ( $H_c = 0$ ). With an increase in the cobalt content, the coercive force increases to  $H_c \approx 95$  Oe.

The results obtained in this article indicate that phase composition and structure are the decisive factors influencing the electromagnetic properties of nanocomposites.

In our future work, we intend to investigate the effects of the annealing process and low temperature on the structural phase and electromagnetic properties of  $\text{Co}_x(\text{MgF}_2)_{100-x}$  nanocomposites.

**Author Contributions:** E.P.D. and E.A.G. conceived and designed the experiments and analyzed the data; S.A.I., P.V.S., D.L.G., K.A.B. and S.V.R. conceived and designed the experiments; A.V.S. contributed the materials. All authors have read and agreed to the published version of the manuscript.

**Funding:** The work was partially supported by the Ministry of Science and Higher Education of the Russian Federation as part of the state task for Universities in the field of scientific activity for 2020–2022, project No. FZGU-2023-0006. The study was supported by the Ministry of Science and Higher Education of Russia under agreement N 075-15-2021-1351 in the field of materials characterization.

**Data Availability Statement:** Data obtained by request.

**Conflicts of Interest:** The authors declare no conflict of interest.

#### References

1. Abeles, B.; Sheng, P.; Coutts, M.D.; Arie, Y. Structural and electrical properties of granular metal films. *Adv. Phys.* **1975**, *24*, 407–461. [[CrossRef](#)]
2. Helman, J.S.; Abeles, B. Tunneling of Spin-Polarized Electrons and Magnetoresistance in Granular Ni Films. *Phys. Rev. Lett.* **1976**, *37*, 1429–1433. [[CrossRef](#)]
3. Meilikhov, E.Z. Tunneling magnetoresistance and Hall effect of granular ferromagnetic metals. *Jetp Lett.* **1999**, *69*, 623–629. [[CrossRef](#)]
4. Tang, J.; Feng, L.; Wiemann, J.A. Negative magnetoresistance of  $\gamma\text{-Fe}_2\text{O}_3$  observed in  $\gamma\text{-Fe}_2\text{O}_3/\text{Ag}$  granular nanocomposites. *Appl. Phys. Lett.* **1999**, *74*, 2522–2524. [[CrossRef](#)]
5. Inoue, M.; Matsumoto, K.; Arai, K.I.; Fujii, T.; Abe, M. Preparation and properties of magneto-optical micro-cavities composed of Co thin film and dielectric multilayers. *J. Magn. Magn. Mat.* **1999**, *196–197*, 611–613. [[CrossRef](#)]
6. Berkowitz, A.E.; Mitchell, J.R.; Carey, M.J. Giant magnetoresistance in heterogeneous Cu-Co alloys. *Phys. Rev. Lett.* **1992**, *68*, 3745–3748. [[CrossRef](#)] [[PubMed](#)]
7. Kijima-Aoki, H.; Cao, Y.; Kobayashi, N.; Takahashi, S.; Ohnuma, S.; Masumoto, H. Large magnetodielectric effect based on spin-dependent charge transfer in metal–insulator type Co-(BaF<sub>2</sub>) nanogranular films. *J. Appl. Phys.* **2020**, *128*, 133904. [[CrossRef](#)]
8. Husain, S.; Barwal, V.; Kumar, N.; Hait, S.; Chaudhary, S. Tunable magnetic anisotropy in obliquely sputtered  $\text{Co}_{60}\text{Fe}_{40}$  thin films on Si(100). *Phys. B Condens. Matter* **2019**, *570*, 1–5. [[CrossRef](#)]
9. Fujimori, H.; Mitani, S.; Ohnuma, S. Tunnel-type GMR in metal-nonmetal granular alloy thin films. *Mater. Sci. Eng. B* **1995**, *31*, 219–223. [[CrossRef](#)]

10. Morikawa, T.; Suzuki, M.; Taga, Y. Soft magnetic properties of Co–Cr–O granular films. *J. Appl. Phys.* **1998**, *83*, 6664–6666. [[CrossRef](#)]
11. Yakushiji, K.; Mitani, S.; Takanashi, K. Composition dependence of particle size distribution and giant magnetoresistance in Co–Al–O granular films. *JMMM* **2000**, *212*, 75–81. [[CrossRef](#)]
12. Zvezdin, A.K.; Kotov, V.A. *Modern Magneto-optics and Magneto-optical Materials*; Institute of Physics Publishing Ltd.: London, UK, 1997.
13. Kravets, V.G.; Petford-Long, A.K.; Kravets, A.F. Optical and magneto-optical properties of  $(\text{CoFe})_x(\text{HfO}_{21})_{1-x}$  magnetic granular films. *J. Appl. Phys.* **2000**, *87*, 1762–1768. [[CrossRef](#)]
14. Gan'shina, E.A.; Kim, C.G.; Kim, C.O.; Kochneva, M.Y.; Perov, N.Y.; Sheverdyayeva, P.A. Magnetostatic and magneto-optical properties of Co-based amorphous ribbons. *J. Magn. Magn. Mater.* **2002**, *239*, 484–486. [[CrossRef](#)]
15. Gan'shina, E.A.; Vashuk, M.V.; Vinogradov, A.N.; Granovsky, A.B.; Gushchin, V.S.; Shcherbak, P.N.; Kalinin, Y.E.; Sitnikov, A.V.; Kim, C.-O.; Kim, C.G. Evolution of the optical and magneto-optical properties in amorphous metal-insulator nanocomposites. *J. Exp. Theor. Phys.* **2004**, *98*, 1027–1036. [[CrossRef](#)]
16. Buravtsova, V.E.; Guschin, V.S.; Kalinin, Y.E.; Kirov, S.; Lebedeva, E.; Phonghirun, S.; Sitnikov, A.; Syr'ev, N.; Trofimenko, I. Magneto-optical properties and FMR in granular nanocomposites  $(\text{Co}_{84}\text{Nb}_{14}\text{Ta}_2)_x(\text{SiO}_2)_{100-x}$ . *CEJP* **2004**, *2*, 566–578. [[CrossRef](#)]
17. Gridnev, S.A.; Kalinin, Y.E.; Sitnikov, A.V.; Stogney, O.V. *Nonlinear Phenomena in Nano—And Microheterogeneous Systems*; BINOM Knowledge Laboratory: Moscow, Russia, 2015.
18. Kobayashi, N.; Ohnuma, S.; Masumoto, T.; Fujimori, H. (Fe–Co)–(Mg-fluoride) insulating nanogranular system with enhanced tunnel-type giant magnetoresistance. *J. Appl. Phys.* **2001**, *90*, 4159–4162. [[CrossRef](#)]
19. Cao, Y.; Umetsu, A.; Kobayashi, N.; Ohnuma, S.; Masumoto, H. Tunable frequency response of tunnel-type magneto-dielectric effect in Co–MgF<sub>2</sub> granular films with different content of Co. *Appl. Phys. Lett.* **2017**, *111*, 122901. [[CrossRef](#)]
20. Tuan, N.A.; Tue, N.A.; Khanh, H.Q. Preparation and electrical characterization of MES-type magnetodielectric system based on Co–Al–O nanogranular films. *J. Mater. Sci. Mater. Electron.* **2021**, *32*, 15643–15652. [[CrossRef](#)]
21. Kimura, M.; Cao, Y.; Kijima-Aoki, H.; Kobayashi, N.; Ohnuma, S.; Masumoto, H. Tunneling Magnetodielectric Effect in Co–Al<sub>2</sub>O<sub>3</sub> Granular Films. *Mater. Trans.* **2022**, *63*, 1677–1681. [[CrossRef](#)]
22. Cao, Y.; Kobayashi, N.; Ohnuma, S.; Masumoto, H. Tunnel-type magneto-dielectric effect and its annealing study in Co–SiO<sub>2</sub> granular films. *Mater. Trans.* **2018**, *59*, 585–589. [[CrossRef](#)]
23. Cao, Y.; Kobayashi, N.; Zhang, Y.-W.; Ohnuma, S.; Masumoto, H. Enhanced spin-dependent charge transport of Co–(Al-fluoride) granular nanocomposite by co-separate sputtering. *J. Appl. Phys.* **2017**, *122*, 133903. [[CrossRef](#)]
24. Xie, F.; Zhang, Y.; Wu, Z.; Qin, Z.; Ji, H.; Liu, X.; Hu, W. Effect of nonuniform microstructure on magnetoresistance and field sensitivity in Co–MgO nanocomposite films. *Vacuum* **2022**, *200*, 110976. [[CrossRef](#)]
25. Domashevskaya, E.P.; Ivkov, S.A.; Sitnikov, A.V.; Stogney, O.V.; Kozakov, A.T.; Nikol'skii, A.V. Formation of nanocrystals of a metal or dielectric component depending on their relative content in  $\text{Co}_x(\text{MgF}_2)_{1-x}$  composites. *Solid State Phys.* **2019**, *61*, 71–79. [[CrossRef](#)]
26. Stogney, O.V.; Sitnikov, A.V.; Kalinin, Y.E.; Avdeev, S.F.; Kopytin, M.N. Isotropic positive magnetoresistance in Co–Al<sub>2</sub>O<sub>n</sub> nanocomposites. *Phys. Solid State* **2007**, *49*, 164–170. [[CrossRef](#)]
27. Barsoukov, E.E.; Macdonald, J.R. *Impedance Spectroscopy: Theory, Experiment, and Applications*; Wiley: New York, NY, USA, 2005; 606p. [[CrossRef](#)]
28. Poklonsky, N.A.; Gorbachuk, N.I. *Fundamentals of Impedance Spectroscopy of Composites: A Course of Lectures*; Belaruce State University: Minsk, Belarus, 2005; 130p.
29. Domashevskaya, E.P.; Ivkov, S.A.; Sitnikov, A.V.; Stogney, O.V. The features of CoFeZr alloy nanocrystals formation in film composites of  $(\text{CoFeZr})_x(\text{MgF}_2)_{100-x}$ . *J. Alloys Compd.* **2021**, *870*, 159398. [[CrossRef](#)]
30. Ganshina, E.A.; Garshin, V.V.; Pripechenkov, I.M.; Ivkov, S.A.; Sitnikov, A.V.; Domashevskaya, E.P. Effect of phase transformations of a metal component on the magneto-optical properties of thin-films nanocomposites  $(\text{CoFeZr})_x(\text{MgF}_2)_{100-x}$ . *Nanomaterials* **2021**, *11*, 1666. [[CrossRef](#)] [[PubMed](#)]
31. Wang, W.; Yang, Y.; Naganuma, H.; Ando, Y.; Yu, R.C.; Han, X.F. The perpendicular anisotropy of Co<sub>40</sub>Fe<sub>40</sub>B<sub>20</sub> sandwiched between Ta and MgO layers and its application in CoFeB/MgO/CoFeB tunnel junction. *Appl. Phys. Lett.* **2011**, *99*, 012502. [[CrossRef](#)]
32. Wang, J.; Pesquera, D.; Mansell, R. Giant non-volatile magnetoelectric effects via growth anisotropy in Co<sub>40</sub>Fe<sub>40</sub>B<sub>20</sub> films on PMN-PT substrates. *Appl. Phys. Lett.* **2019**, *114*, 092401. [[CrossRef](#)]

**Disclaimer/Publisher's Note:** The statements, opinions and data contained in all publications are solely those of the individual author(s) and contributor(s) and not of MDPI and/or the editor(s). MDPI and/or the editor(s) disclaim responsibility for any injury to people or property resulting from any ideas, methods, instructions or products referred to in the content.